α-resonance structure in ^{11}C studied via resonant scattering of ^{7}Be + α and with the ^{7}Be(α, p) reaction

H. Yamaguchi (山口英斉)* and D. Kahl
Center for Nuclear Study, the University of Tokyo, RIKEN Campus, 2-1 Hirosawa, Wako, Saitama 351-0198, Japan

Y. Wakabayashi (若林 泰生) and S. Kubono (久保野 茂)
The Institute of Physical and Chemical Research (RIKEN), 2-1 Hirosawa, Wako, Saitama 351-0198, Japan

T. Hashimoto (橋本 尚志)
Research Center for Nuclear Physics, Osaka University, 10-1 Mihogaoka, Ibaraki, Osaka 567-0047, Japan

S. Hayakawa (早川 勢也)
Laboratori Nazionali del Sud, Istituto Nazionale di Fisica Nucleare, Via S. Sofia 62, 95125 Catania, Italy

T. Kawabata (川畑 貴裕)
Department of Physics, Kyoto University, Kita-Shirakawa, Kyoto 606-8502, Japan

N. Iwasa (岩佐 直仁)
Department of Physics, Tohoku University, Aoba, Sendai, Miyagi 980-8578, Japan

T. Teranishi (寺西 高)
Department of Physics, Kyushu University, 6-10-1 Hakozaki, Fukuoka 812-8581, Japan

Y. K. Kwon (권영관)
Institute for Basic Science, 70, Yuseong-daero 1689-gil, Yuseong-gu, Daejeon 305-811, Korea

D. N. Binh, L. H. Khiem, and N. N. Duy
Institute of Physics, Vietnam Academy of Science and Technology, 18 Hong Quoc Viet, Nghia do, Hanoi, Vietnam
(Received 21 December 2012; published 4 March 2013)

Background: The resonance structure in ^{11}C is of particular interest with regard to the astrophysical ^{7}Be(α,γ) reaction, relevant at high temperature, and to the α-cluster structure in ^{11}C.
Purpose: The measurement was made to determine the unknown resonance parameters for the high excited states of ^{11}C. In particular, the α-decay width can be useful information to discuss the α-cluster structure in ^{11}C.
Methods: New measurements of ^{7}Be + α resonant scattering and the ^{7}Be(α, p)^{10}B reaction in inverse kinematics were performed for center-of-mass energy up to 5.5 MeV, and the resonances at excitation energies of 8.9–12.7 MeV in the compound ^{11}C nucleus were studied. Inelastic scattering of ^{7}Be + α and the ^{7}Be(α, p_1)^{10}B* reaction were also studied with a simultaneous γ-ray measurement. The measurements were performed at the low-energy radioactive ion beam facility CRIB (CNS Radioactive Ion Beam separator) of the Center for Nuclear Study, the University of Tokyo.
Results: We obtained excitation functions of ^{7}Be(α,α_0)^{7}Be (elastic scattering), ^{7}Be(α,α_1)^{7}Be* (inelastic scattering), ^{7}Be(α, p_0)^{10}B, and ^{7}Be(α, p_1)^{10}B*. Many resonances including a new one were observed and their parameters were determined by using an R-matrix analysis.
Conclusions: The resonances we observed possibly enhance the ^{7}Be(α,γ) reaction rate but with a smaller magnitude than the lower-lying resonances. A new negative-parity cluster band, similar to the one previously suggested in the mirror nucleus ^{11}B, is proposed.

DOI: 10.1103/PhysRevC.87.034303 PACS number(s): 25.55.−e, 24.30.−v, 21.60.Gx, 27.20.+n

I. INTRODUCTION

The ^{7}Be(α,γ)^{11}C reaction is considered to play an important role in the hot *pp* chain and related reaction sequences [1]. Several reaction sequences including the ^{7}Be(α,γ)^{11}C reaction should take place in some high-temperature environments. One of those sequences is called *pp*-V,

$$^{7}\mathrm{Be}(\alpha,\gamma)^{11}\mathrm{C}(\beta^{+}\nu)^{11}\mathrm{B}(p,2\alpha)^{4}\mathrm{He}.$$

Others are breakout processes called rap (II, III, and IV),

$$^{7}\mathrm{Be}(\alpha,\gamma)^{11}\mathrm{C}(p,\gamma)^{12}\mathrm{N}(p,\gamma)^{13}\mathrm{O}(\beta^{+}\nu)^{13}\mathrm{N}(p,\gamma)^{14}\mathrm{O},$$
$$^{7}\mathrm{Be}(\alpha,\gamma)^{11}\mathrm{C}(p,\gamma)^{12}\mathrm{N}(\beta^{+}\nu)^{12}\mathrm{C}(p,\gamma)^{13}\mathrm{N}(p,\gamma)^{14}\mathrm{O},$$

*yamag@cns.s.u-tokyo.ac.jp

and

$$^{7}\mathrm{Be}(\alpha,\gamma)^{11}\mathrm{C}(\alpha,p)^{14}\mathrm{N}(p,\gamma)^{15}\mathrm{O},$$

which are reaction chains to synthesize CNO nuclei without the triple-α process, effective at $T_9 > 0.2$, where T_9 is the temperature in gigakelvins. At T_9 below 0.2, ^{7}Be predominantly makes an electron capture, almost independent of the density. The $^{7}\mathrm{Be}(\alpha,\gamma)^{11}\mathrm{C}$ reaction and these sequences possibly play important roles in the explosion of supermassive objects with lower metallicity [2], novae [3], and big-bang nucleosynthesis [4,5]. The $^{7}\mathrm{Be}(\alpha,\gamma)^{11}\mathrm{C}$ reaction rate is greatly affected by the resonances. At the lowest temperature, there is a large contribution to the reaction rate from the subthreshold resonance at the excitation energy $E_{\mathrm{ex}} = 7.50$ MeV. The two resonances located at $E_{\mathrm{ex}} = 8.11$ MeV and $E_{\mathrm{ex}} = 8.42$ MeV determine the rate at higher temperature around $T_9 = 0.5$–1. Higher excited states may contribute to the reaction rates at $T_9 > 1$. A recent theoretical calculation [6] of the νp-process in core-collapse supernovae [7] shows that the $^{7}\mathrm{Be}(\alpha,\gamma)$ reaction may contribute as much as the triple-α process to the synthesis of elements heavier than boron at the relevant temperature of $T_9 = 1.5$–3. Therefore, it is also important to study the resonances for such a high-temperature region, corresponding to $E_{\mathrm{ex}} \sim 8$–10 MeV in the Gamow energy window.

Information on the excited states in ^{11}C is still limited. Resonance states above $E_{\mathrm{ex}} = 9$ MeV have been studied via $^{10}\mathrm{B}(p,\alpha)$ and other reactions such as $^{12}\mathrm{C}(p,d)^{11}\mathrm{C}$ [8–17]. The resonances typically have widths of the order of 100 keV, but their α-decay widths Γ_α are not known with good precision, and even the spin and parity (J^π) have not yet been clearly determined for some of the states. The excited states at lower energies ($E_{\mathrm{ex}} = 8$–9 MeV) have narrower particle widths, and Γ_α values are only known for two resonances located at $E_{\mathrm{ex}} = 8.11$ and 8.42 MeV. The $^{7}\mathrm{Be}(\alpha,\gamma)^{11}\mathrm{C}$ reaction cross section was directly measured only at the energies of these two resonances [18].

Another point of interest for the $^{7}\mathrm{Be}+\alpha$ system is its nuclear cluster structure. The $3/2^-_3$ state in ^{11}C at $E_{\mathrm{ex}} = 8.11$ MeV is regarded as a dilute cluster state similar to the one in ^{12}C [19], where two α particles and ^{3}He are weakly interacting and spatially extended. Its exotic structure is attracting much attention [20]. The cluster structure in ^{11}B, the mirror nucleus of ^{11}C, was studied by measuring its isoscalar monopole and quadrupole strengths in the $^{11}\mathrm{B}(d,d')$ reaction [21,22], and results indicated that the 8.56-MeV state in ^{11}B, the mirror of the 8.11-MeV state in ^{11}C, has a dilute cluster structure. Besides this state, rotational bands in ^{11}B and ^{11}C, which might be related to the α-cluster structure, have been discussed [23,24]. In our recent study of ^{11}B using $^{7}\mathrm{Li}+\alpha$ resonant elastic scattering, we observed strong α resonances, and we determined their Γ_α values. A new cluster band with negative parity was also suggested in the highly excited states [25].

In the present study, we performed a measurement of the $^{7}\mathrm{Be}+\alpha$ resonant elastic scattering to study resonance structure of ^{11}C, complementary to the previous study [25]. We also measured protons from $^{7}\mathrm{Be}(\alpha,p)^{10}\mathrm{B}$ reactions, which have been studied mostly by its inverse reaction. The actual measurements were performed in inverse kinematics, $^{4}\mathrm{He}(^{7}\mathrm{Be},\alpha)$ and $^{4}\mathrm{He}(^{7}\mathrm{Be},p)$, but we denote these as $^{7}\mathrm{Be}(\alpha,\alpha)$ and $^{7}\mathrm{Be}(\alpha,p)^{10}\mathrm{B}$ for consistency. The strengths of the resonances in the present study should provide useful information on the α-cluster structure of ^{11}C and on the astrophysical $^{7}\mathrm{Be}(\alpha,\gamma)$ reaction rate. Recently, a similar measurement independently planned at other facilities was carried out and published by Freer *et al.* [26]. We will present our new results and discuss the differences of the two new measurements. An essential difference is that we have measured γ rays to obtain excitation functions of $^{7}\mathrm{Be}(\alpha,\alpha_1)^{7}\mathrm{Be}^*$ and $^{7}\mathrm{Be}(\alpha,p_1)^{10}\mathrm{B}^*$ reactions, which was not considered in [26].

II. METHOD

The measurements were performed at the low-energy radioactive ion beam facility CRIB (CNS Radioactive Ion Beam separator) [27,28], using the thick-target method in inverse kinematics [29] to obtain excitation functions of elastic scattering and others for $E_{\mathrm{ex}} = 8.7$–13.0 MeV in ^{11}C. The experimental setup is almost identical to the one used in our $^{7}\mathrm{Li}+\alpha$ measurement [25], except that the beam was a radioactive ion beam produced at CRIB. A pure and intense ^{7}Be beam can be produced in-flight at CRIB using a cryogenic gas target [30]. In the present measurement, a ^{7}Be beam was produced using a 2.3-mg/cm^2-thick hydrogen gas target and a ^{7}Li beam at 5.0 MeV/u accelerated with the AVF cyclotron of RIKEN. By using an 8.5-μm Havar foil as an energy degrader after the beam-production target, a low-energy ^{7}Be beam at 17.9 MeV was produced. The ^{7}Be beam was separated and purified by using magnetic analysis and velocity selection with a Wien filter. The purity of the ^{7}Be beam was about 30% and almost 100% before and after the Wien filter, respectively. The experimental setup after the Wien filter is shown in Fig. 1. The beam collimator was a 20 × 20 mm rectangular aperture, accepting a large fraction of the transported beam.

A micro-channel plate (MCP) was used for the detection of the beam position and timing. A CsI-deposited 0.7-μm-thick aluminum foil was placed on the beam axis for the secondary electron emission. The secondary electrons were accelerated along the beam axis and reflected by 90° at a biased thin-wire reflector and detected at the MCP with a two-dimensional delay-line readout.

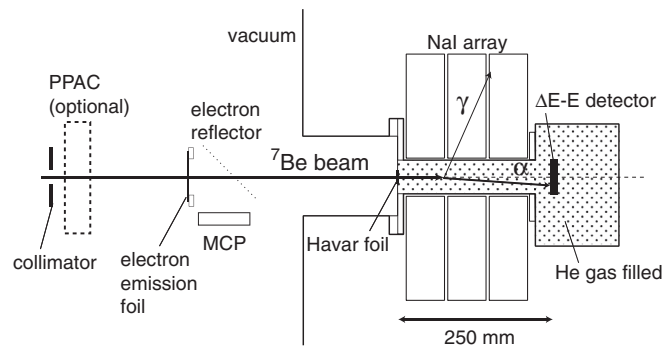

FIG. 1. Experimental setup of the measurement of $^{7}\mathrm{Be}+\alpha$ elastic scattering and others in inverse kinematics.

The gas target consisted of a 50-mm-diameter duct and a subsequent small chamber. Helium gas at 815 Torr was added to the chamber, which was sealed with a 2.5-μm-thick Havar foil as the beam entrance window. The ^{7}Be beam energy after the entrance window of the helium gas target was measured as 15.43 ± 0.13 MeV. α particles recoiling to forward angles were detected by the ΔE-E detector. The detector, consisting of 20-μm- and 490-μm-thick silicon detectors, was placed in the gas chamber. The helium gas was sufficiently thick to stop the ^{7}Be beam before it reached the ΔE-E detector. The distance from the beam entrance window to the detector was 250 mm. Each detector had an active area of 50×50 mm, and 16 strips for one side, making pixels of 3×3 mm. These detectors were calibrated with α sources, as well as with proton and α beams at various energies produced during the run. Each detector had an energy resolution better than 1.5% in full width at half maximum (FWHM) for 5-MeV α particles. The measurement using the proton and α beams was also for the evaluation of the dead-layer thickness between the two detectors. To measure 429-keV γ rays from inelastic scattering to the first excited state of ^{7}Be, ten NaI(Tl) detectors were placed around the duct and each NaI(Tl) crystal had a geometry of $50 \times 50 \times 100$ mm. They covered 20%–60% of the total solid angle, depending on the reaction position in the long target. The energy-dependent photopeak efficiency of the NaI array was measured at various positions in the gas target, using standard radioactive sources of ^{137}Cs, ^{22}Na, and ^{60}Co. The efficiency was determined as 15%–30% for 429-keV γ rays. The energy resolution was about 9% in FWHM against 662-keV γ rays.

Most of the particles measured at the ΔE-E detector were α particles from elastic scattering and protons from the ^{7}Be(α, p) reaction. Some are in coincidence with γ rays, as shown later. The typical ^{7}Be beam intensity used in the measurement was 2×10^5 particles per second at the secondary target, and the main measurement using the helium-gas target was performed for 4 days, injecting 2.9×10^{10} ^{7}Be particles into the gas target. We performed another measurement using an argon-gas target of an equivalent thickness for 1 day to evaluate the background α particles reaching the ΔE-E detector as a contamination in the secondary beam.

To obtain a correct cross section with the current thick-gas target method, one needs a correct reaction position, which is determined by the geometrical information of the target and detector and energy loss of the beam and α particles. A measurement with a parallel-plate avalanche counter (PPAC) [31] in addition to the MCP was also performed for a short time to check whether the cross section is consistent between two measurements with different reaction positions for the same $E_{\mathrm{c.m.}}$. In that measurement, the ^{7}Be beam energy after the entrance window was degraded to 12.2 MeV, due to the additional energy loss in the PPAC. As a result, the reaction position is shifted by 6 cm at maximum to the upstream direction, which also makes the solid angle smaller, as compared with the measurement with the MCP alone. We confirmed that the cross sections finally obtained for both measurements were in good agreement, showing that there is no large error in the determination of the reaction position.

III. DEDUCTION OF EXCITATION FUNCTIONS

A. Particle identification

The particle identification performed with the ΔE-E detector for the helium and argon target measurements are shown separately as two-dimensional energy plots in Fig. 2, where the total energy deposition of particles is plotted against the energy deposition in the ΔE counter. As illustrated, α particles and protons were clearly separated. In the background run with argon gas, we observed non-negligible numbers of protons and α particles as shown in Fig. 2(b). They are considered as beamlike particles produced at the production target as contaminants in the ^{7}Be beam, and they reached the silicon detectors at the end of the beamline. Most such particles should have been eliminated at the Wien filter, but a very small number comparable to the reaction products remained, possibly because of scattering in the inner wall of the beamline or for some other reason.

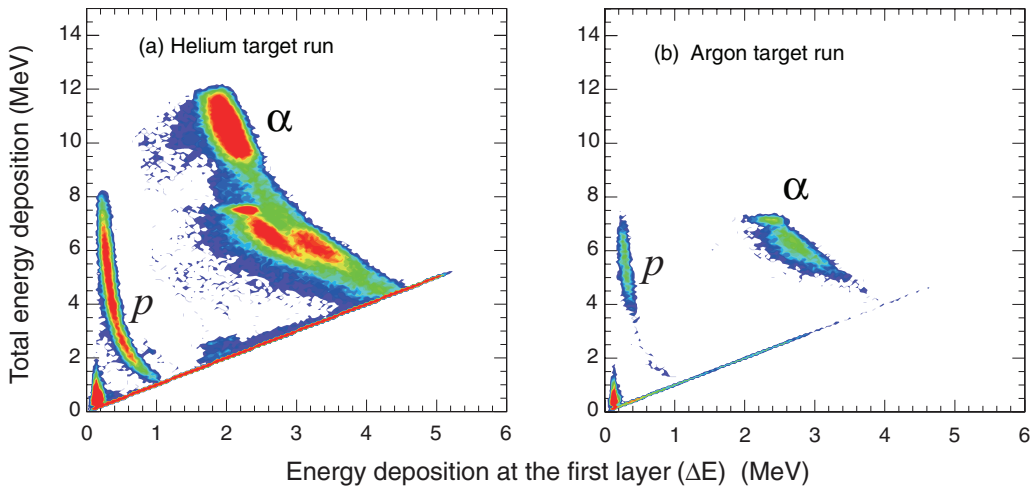

FIG. 2. (Color online) ΔE-E plot for the particle identification.

In Fig. 2(a), one may notice the locus of α particles branched at a total energy about 6 MeV. This branching is possibly attributed to the channeling effect [32,33] of the thin silicon detector. In the background run, shown in Fig. 2(b), only the left branch was prominent, which implies that background α particles coming from upstream comprise the left branch. We observed events in the background run also at the right branch, but the number was much smaller than for the left branch. Such α particles had a strict limitation on the incoming angle, which was almost perpendicular to the surface of the silicon detector, and thus the channeling effect could be most prominent. On the other hand, α particles from real scattering events had a broader range of angles and are less susceptible to the channeling effect. Although there was such a branching, we successfully evaluated the amount of background events by using an argon-target measurement, which we then subtracted from the the helium-target measurement data. Performing the argon-target measurement was useful not only for the background evaluation but also for understanding the unexpected origin of branching in the α particles.

B. Calculation of cross section

The energy of the ^{7}Be beam at any position in the gas target was obtained with a good center-of-mass energy $E_{\mathrm{c.m.}}$ resolution (70 keV or better), based on a direct energy measurement at seven different target pressures, compared with an energy loss calculation using the SRIM [34] code. Using this energy loss function, the energy of a recoiled α particle measured by the ΔE-E detector was converted to $E_{\mathrm{c.m.}}$, by calculating the kinematical relationship for elastic scattering. We selected events with an α particle in coincidence with a ^{7}Be beam particle measured in a 20 $\times$ 20 mm square at the center of the MCP. The scattering angle determined from the detection position of the ΔE-E detector was used in the kinematical calculation as a correction. The energy loss of the recoiled α particle in the gas target was calculated by using SRIM and also considered in the calculation. The differential cross section $d\sigma/d\Omega$ was calculated for each small energy division using the solid angle of the detector, number of beam particles, and the effective target thickness. The solid angle was calculated by using the geometrical information of the detector and the reaction position in the target determined from the kinematical calculation. The number of beam particles was obtained based on single counting of the beam particle by the MCP, simultaneously recorded in the measurement. Note that it is very important to obtain a correct energy loss function in the target, since the target thickness and the solid angle, both directly reflected in the cross section, were also calculated using the function.

In a similar procedure, but selecting proton events and using the kinematical relationship of the ^{7}Be$(\alpha,p)^{10}$B reaction, we obtained a spectrum containing ^{7}Be$(\alpha,p)^{10}$B reaction events.

Events of inelastic scattering ^{7}Be$(\alpha,\alpha_1)^7$Be* producing ^{7}Be* at the first excited state were identified by measuring 429-keV γ rays with the NaI array. We selected triple-coincidence events in which a ^{7}Be beam particle was detected at the beam detector (MCP), an α or any other particle was detected at the silicon detectors, and a γ ray was detected at the NaI array. The γ-ray energy spectrum for those events is shown in Fig. 3. The peak at 429 keV was clearly identified, and small peaks around 511 and 718 keV, which should be from positron annihilations and excited ^{10}B* produced via the ^{7}Be$(\alpha,p_1)^{10}$B* reaction, respectively, were also observed. We performed a finer event discrimination by taking events in which an α particle was identified, the beam is hitting the central part of the MCP, and an energy spectrum of γ rays with a good signal-to-noise ratio was obtained, as shown in the inset of Fig. 3. The events with a 429-keV γ ray were used to obtain the excitation function of inelastic scattering. A similar event discrimination was successfully performed for protons, as also shown in the inset of the figure, to select events of the ^{7}Be$(\alpha,p_1)^{10}$B* reaction. The photopeak efficiency of the NaI array, measured at various positions in the gas target, was used for the calculation of the absolute cross section. Finally, excitation functions of inelastic scattering and the ^{7}Be$(\alpha,p_1)^{10}$B* reaction were obtained.

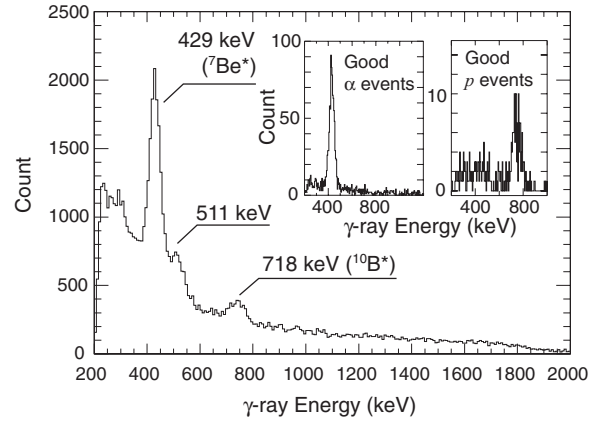

FIG. 3. Energy spectrum of γ rays for ^{7}Be-α-γ triple-coincidence events. The insets show the same spectrum for events with an α particle or p identified, after a beam position selection.

C. Background subtraction

The ^{7}Be$(\alpha,\alpha)^7$Be and ^{7}Be$(\alpha,p)^{10}$B spectra obtained by using the above procedure still contain background α and p contributions, the amount of which could be evaluated from the argon-target measurement. The background contribution to the differential cross sections were evaluated as shown in Fig. 4.

The sharp peak at 3.7 MeV in the background α spectrum corresponds to α particles which had their magnetic rigidity analyzed at the dipole magnets (D1 and D2) in CRIB. The broader lower-energy component is possibly from α particles which had the same origin but were scattered somewhere along the beamline. The heights of the sharp peak for both target runs are in good agreement, but the broad component was significantly higher in the helium-target spectrum. This suggests that the peak around 3–3.5 MeV observed in the helium-target spectrum is partially due to the background α particles, but the rest is contributed by real scattering events. By subtracting the background contribution and the

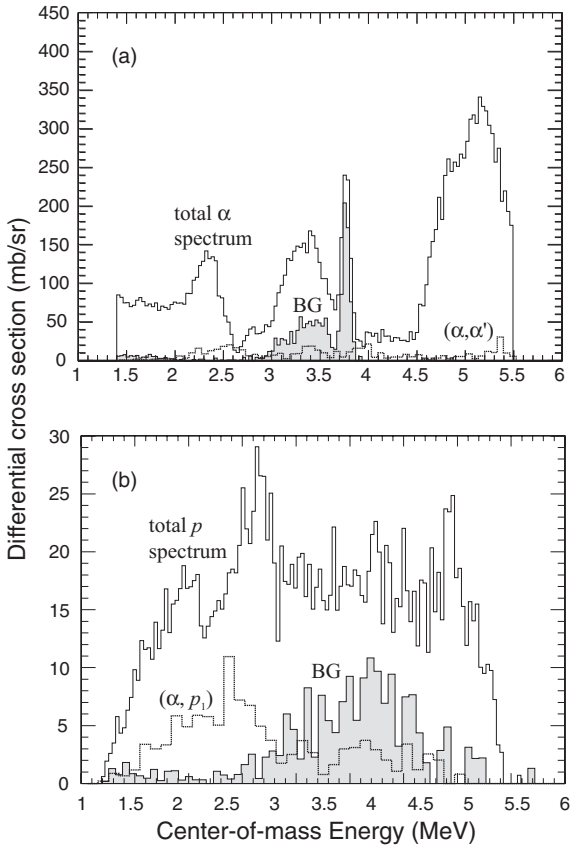

FIG. 4. Background subtraction for (a) α and (b) p spectra. Total α and p spectra are the excitation functions of ^{7}Be$(\alpha,\alpha)^{7}$Be and ^{7}Be$(\alpha,p)^{10}$B, but still containing background events. Shaded spectra show the contributions of background α and p as beam contaminations. The spectra of ^{7}Be$(\alpha,\alpha_1)^{7}$Be* and ^{7}Be$(\alpha,p_1)^{10}$B* are also shown.

contribution of inelastic scattering events, we obtained an excitation function of elastic scattering.

There was no sharp peak in the background proton spectrum, but we performed a similar subtraction for the broad background and obtained the ^{7}Be$(\alpha,p)^{10}$B spectrum. The contribution from the ^{7}Be$(\alpha,p_1)^{10}$B* reaction was also considered. Finally, we obtained excitation functions for four different cross sections, ^{7}Be$(\alpha,\alpha_0)^{7}$Be, ^{7}Be$(\alpha,\alpha_1)^{7}$Be*, ^{7}Be$(\alpha,p_0)^{10}$B, and ^{7}Be$(\alpha,p_1)^{10}$B*. We refer to these excitation functions as the α_0, α_1, p_0, and p_1 spectra, respectively, in the following sections. The excitation functions are shown in Fig. 5. The peak structure observed in the excitation functions should correspond to the resonances in ^{11}C. The curves are fitted curves by using an R-matrix analysis, which will be described later.

D. Energy and angular uncertainty

Uncertainty in $E_{\mathrm{c.m.}}$ and average center-of-mass scattering angle $\theta_{\mathrm{c.m.}}$ are plotted for the α_0 and p_0 spectra in Fig. 6, and the curves for α_1 and p_1 spectra are quite similar to those.

For the α_0 spectrum, the overall uncertainty in $E_{\mathrm{c.m.}}$ was estimated as 70–130 keV, depending on the energy. The uncertainty mainly originated from the energy straggling of the ^{7}Be beam and α particles (30–80 keV), the energy resolution of the ΔE-E detector (20–55 keV), and the angular uncertainty due to the finite size of the detector (20–100 keV). The uncertainty is similar for the α_1 spectrum and slightly better for the p_0 and p_1 spectra.

The excitation functions in Fig. 5 are for certain angular range covering $\theta_{\mathrm{c.m.}} = 180^\circ$. The average $\theta_{\mathrm{c.m.}}$ was 167° at $E_{\mathrm{c.m.}} = 3$ MeV, but it depends on $E_{\mathrm{c.m.}}$. The dependence is because the ΔE-E detector and the long helium gas target were closely arranged to obtain good statistics, and we had to select events within a fixed area of the detector in the analysis.

IV. COMPARISON WITH PREVIOUS RESULTS

A. Comparison with previous inverse reaction measurements

A direct comparison is possible for our p_0 spectrum with the previous measurements of the inverse ^{10}B$(p,\alpha)^{7}$Be reaction [11,12,15], although the measured scattering angles are not the same. The laboratory cross sections of the previous measurements were converted into the center-of-mass cross section, using the detailed balance theorem. Figure 7(a) shows the data in [12] at laboratory angle $\theta_{\mathrm{lab}} = 150^\circ$ and the present measurement with an R-matrix calculation. The present measurement had a corresponding average angle in the inverse reaction of $\theta_{\mathrm{lab}} = 164^\circ$ (at $E_{\mathrm{c.m.}} = 3$ MeV). Figure 7(b) shows the data in [11,12,15], all with $\theta_{\mathrm{lab}} = 90^\circ$, but the present measurement data shown are the same as in Fig. 7(a). The curve for the present work is created by using an R-matrix calculation performed with the same resonant parameters as in Fig. 7(a), but with the angle adjusted to these previous measurements.

Given the large uncertainty of our measurement, the overall features of the present spectrum are in agreement with previous measurements, such that the two peaks around 3 and 5 MeV are distinct. The absolute cross section shows a disagreement to some extent, but the previous measurements already had differences from one another as in Fig. 7(b). The cross sections of [11] or [15] show magnitudes similar to ours, but the angle is at $\theta_{\mathrm{lab}} = 90^\circ$. The cross section of [12] at the same angle is lower than these two and our data at $\theta_{\mathrm{lab}} = 164^\circ$. The angular dependence may partly explain the difference, as shown by the R-matrix curves at two different angles. One can see the calculation at $\theta_{\mathrm{lab}} = 90^\circ$ is closer to the data of [12] at $\theta_{\mathrm{lab}} = 90^\circ$. The cross section of the present work at 3.5–4.5 MeV appears higher than any of the previous data and the R-matrix calculation. We did not introduce strong resonances in this region to improve the fitting, since such resonances were not observed in the previous measurements. This discrepancy might be related to the background protons, which were distributed around 3–4.5 MeV, as shown in Fig. 4.

B. Comparison with the latest inverse kinematics measurement

The measurement by Freer *et al.* [26] has been performed with essentially the same method as used in the present work. Here we compare the two results. The α_0 and p_0 spectra of both measurements are compared in Fig. 8. The overall shapes of the two α_0 spectra have a common feature. There is a large double-peak structure around $E_{\mathrm{c.m.}} = 5$ MeV, and

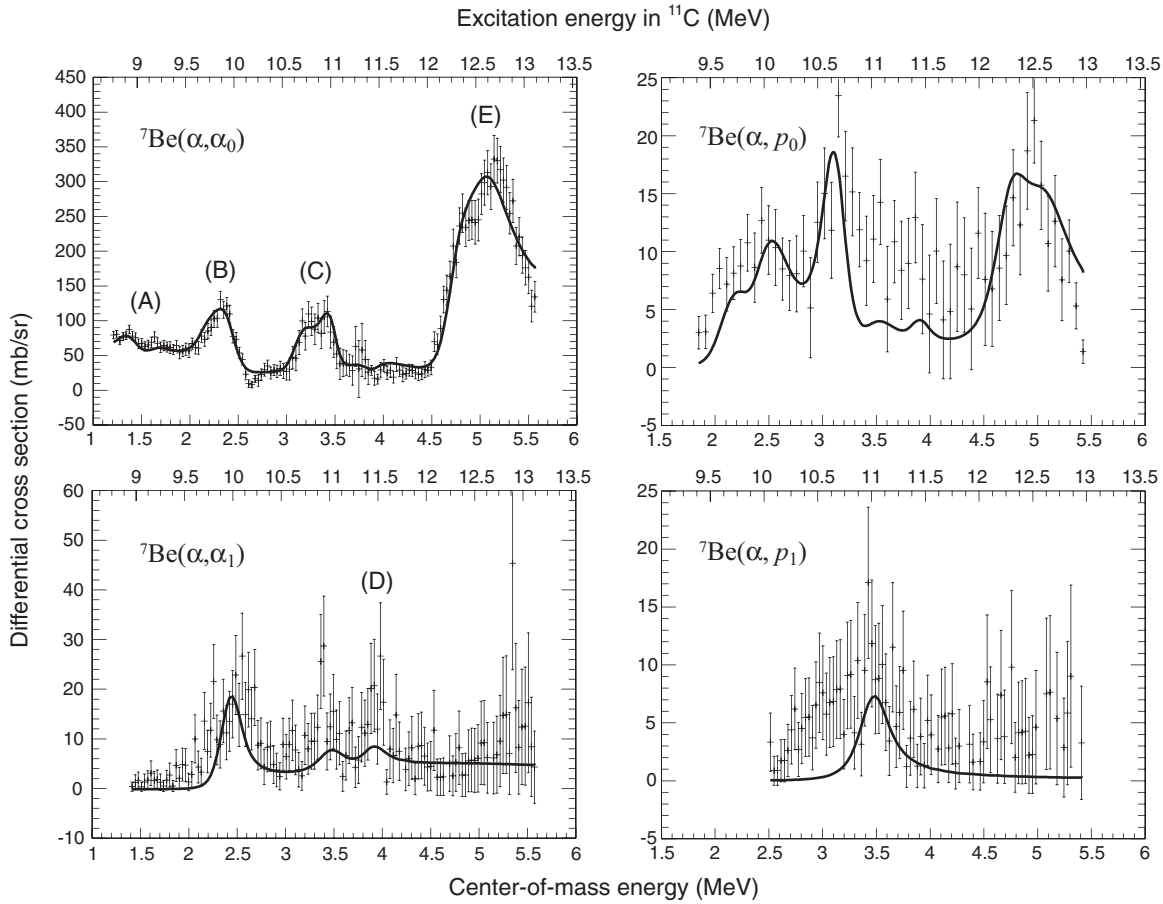

FIG. 5. Excitation functions, referred to as α_0, α_1, p_0, and p_1 spectra. The best-fit curves from the R-matrix analysis are also shown. The labels (A–E) correspond to structures discussed in Sec. V.

smaller peaks are located at an energy 1 MeV below and at lower energies. However, two large differences are seen: the absolute cross section is different by a factor of 2–3 for the higher energy part, and the peaks are displaced in energy by about 500 keV. The cross section in [26] was normalized using the low-energy measurement data, and also by using a Monte Carlo simulation, which may produce a systematic uncertainty of as much as a factor of 2.5 at maximum, as they claim. On the other hand, our cross section is based on single

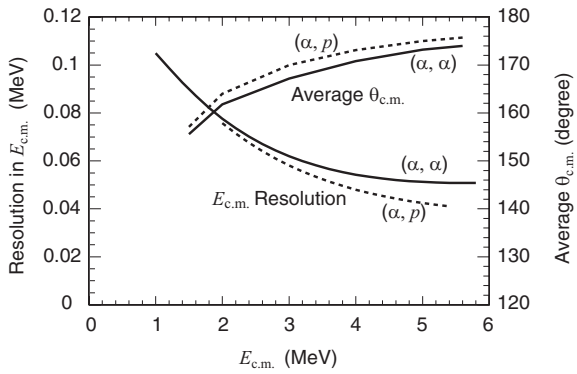

FIG. 6. Uncertainty in $E_{c.m.}$ and averaged $\theta_{c.m.}$ for the α_0 and p_0 spectra.

counting of the beam particles and geometrical measurement. Furthermore, the previous ^{7}Li + α measurement [25] with the same analysis method yielded a consistent cross section with older normal kinematics measurements. Therefore, an error in the cross section by a factor of 2–3 is unlikely to be produced in our measurement or analysis. In the thick-target method, the energy can be easily shifted if the energy loss functions of the ^{7}Be beam or the α particle in the target is not correct. In both our measurements, the energy loss of the beam was directly measured over a wide range of pressures. We used the SRIM code for the energy loss of the α particle, and the higher edge of $E_{c.m.}$ from the measured data (5.5 MeV) was in good agreement with the $E_{c.m.}$ expected from the measured beam energy at the beginning of the target. We do not expect an error in $E_{c.m.}$ of much more than 100 keV at $E_{c.m.} \sim$ 5 MeV. Another fact that may support the present work is that our spectrum could be explained with the known energy level information, as shown later, but in [26] it was necessary to introduce several new resonances to perform an R-matrix fit.

The p_0 spectrum in [26] was separated into two energy regions. The lowest energy part perfectly agree with ours, but the data in [26] at higher energy again show a lower cross section. However, the discrepancy is not obvious, since the deviation is comparable to the uncertainty and is quite large in both measurements.

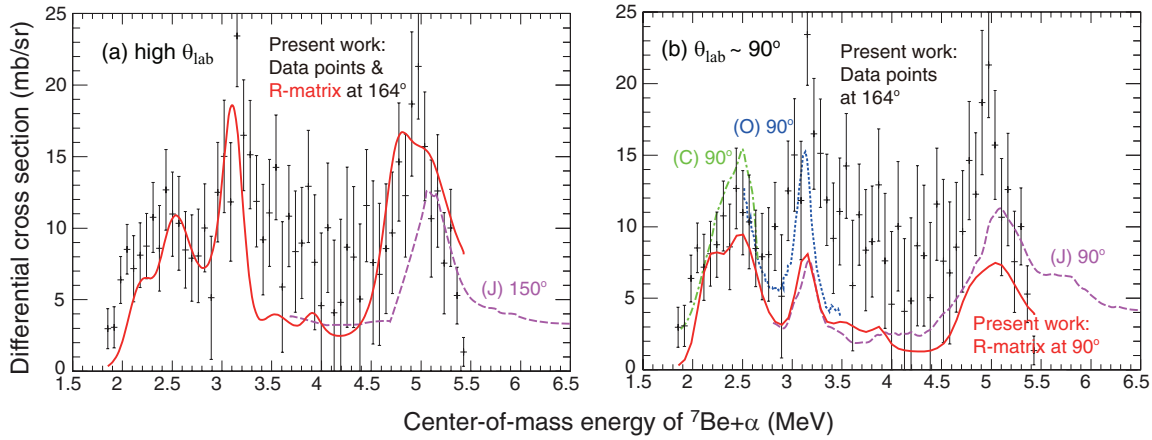

FIG. 7. (Color online) The p_0 spectrum compared with previous measurements of the inverse ^{10}B$(p,\alpha)^7$Be reaction by (J) Jenkin *et al.* [12], (C) Cronin [11], and (O) Overley and Whaling [15]. *R*-matrix calculations performed at $\theta_{\rm lab} = 90^\circ$ and 164° are also shown. Note that the angles are in the laboratory system of the ^{10}B$(p,\alpha)^7$Be reaction.

V. *R*-MATRIX ANALYSIS

Several resonance structures were observed in our α_0 spectrum, namely, (A) two small peaks at 8.9–9.2 MeV, (B) a peak around 10 MeV, (C) a broad peak at 10.5–11.0 MeV, considered to be a doublet, and (E) a doublet structure at 12–13 MeV, as shown in Fig. 5. Structures were also observed in the other three spectra—with some corresponding to the peaks in the α_0 spectrum, and others not—such as (D) a small enhancement of the cross section in the α_1 spectrum at 11.4 MeV.

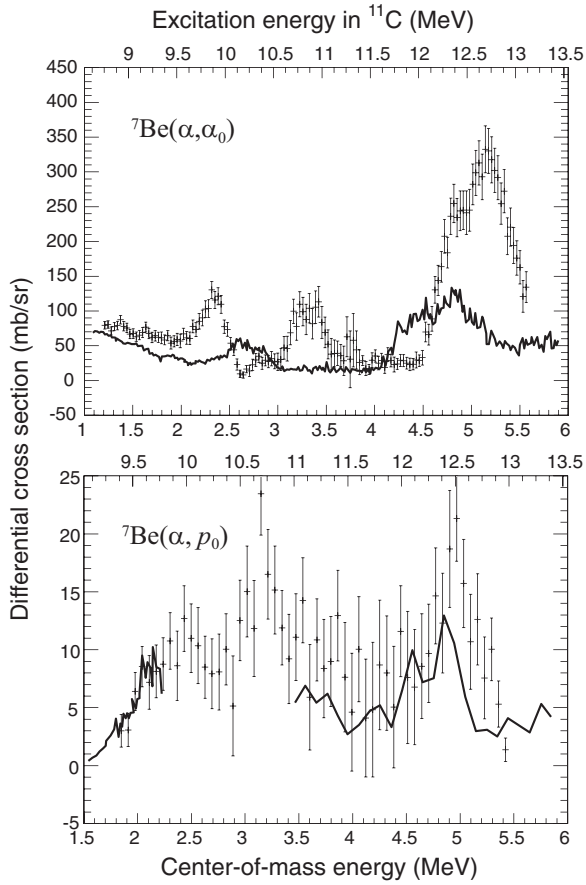

FIG. 8. The α_0 and p_0 spectra from the present work and [26] (solid lines).

We performed an analysis using an *R*-matrix calculation code (SAMMY8 [35]) to deduce resonance parameters. The decay widths of four channels, $\Gamma_{\alpha 0}$, $\Gamma_{\alpha 1}$, Γ_{p0}, and Γ_{p1}, were considered in the *R*-matrix analysis. The basic strategy was as follows. First $\Gamma_{\alpha 0}$ values were roughly determined by an *R*-matrix fit of the α_0 spectrum, reproducing the peak structure. Using the $\Gamma_{\alpha 0}$ values, we analyzed the p_0 spectrum and found the best values for $\Gamma_{\alpha 0}$ and Γ_{p0}. Then, the α_0 spectrum was analyzed again to determine $\Gamma_{\alpha 0}$ more precisely. When $\Gamma_{\alpha 0}$ and Γ_{p0} were determined consistently by using the two spectra, an analysis was performed for the α_1 and p_1 spectra, both of which had low statistics and do not exhibit much structure. By repeating the above process until it converges, all four widths, $\Gamma_{\alpha 0}$, $\Gamma_{\alpha 1}$, Γ_{p0}, and Γ_{p1}, were determined. To cope with the many parameters in the fitting, we adopted resonant parameters from previous measurements [36] as much as possible. The detailed discussions for each structure we observed (A–E), including the J^π determination, are below. Another restriction we considered was that the sum of the decay widths could not exceed the known total width $\Gamma_{\rm tot}$ too much. The calculation was performed with channel radii $R_c = 4.2$ fm for the ^{7}Be + α channel and $R_c = 3.8$ fm for the ^{10}B + p channel. These channel radii were deviated by 20% for the evaluation of the uncertainties. The angle was fixed at $\theta_{\rm c.m.} = 167^\circ$ for the α_0 and α_1 spectra, and $\theta_{\rm c.m.} = 169^\circ$ for the p_0 and p_1.

The results are summarized in Table I. The Wigner limit $\Gamma_w = 2\hbar^2/\mu R^2 P_l$, where μ is the reduced mass and P_l is the penetrability, was calculated for an α particle with an interaction radius $R = 4.2$ fm and shown in the table for comparison. Uncertainties could be reasonably evaluated only for some $\Gamma_{\alpha 0}$, as shown in Table I, and the other widths could have very large uncertainties.

A. Peaks at 8.9–9.2 MeV

In this energy region the excitation function was rather flat in the α_0 spectrum, but two small bumps were observed. One

TABLE I. Best-fit resonance parameters of ^{11}B determined by the present work. The E_{ex} and J^π values shown in italic letters were fixed to those in [36,38], and the others are proposed in the present work. See text for other possible J^π assignments.

E_{ex} (MeV)	J^π	$l_{\alpha 0}$	$\Gamma_{\alpha 0}$ (KeV)	Γ_{p0} (KeV)	$\Gamma_{\alpha 1}$ (KeV)	Γ_{p1} (KeV)	Γ_{tot} [38] (KeV)	$\Gamma_{W\alpha}$ (KeV)
8.90	$(9/2^+)$	3	8					6.4
9.20	$5/2^+$	3	13				500	21
9.65	$(3/2^-)$	0	20	50			210	1310
9.78	$(5/2^-)$	2	19	100			240	450
9.97	$(7/2^-)$	2	153 ± 55	35	30		120	580
10.083	$7/2^+$	3	25	230			230	90
10.679	$9/2^+$	3	58 ± 36	110			200	230
11.03	$(5/2^-)$	3	130 ± 83	25	45	120	300	360
11.44	$(3/2^+)$	1	80	30	150		360	2680
12.40	$9/2^+$	3	460 ± 150	90			1000–2000	1100
12.65	$(7/2^+)$	3	420 ± 178	110			360	1270

of these may correspond to the known $5/2^+$ state at 9.20 MeV [37]. The other one is located around 8.90 MeV. A resonance at this energy is not known from previous measurements and we regard this as a new resonance. However, it could be the same resonance as the one at 8.655 $(7/2^+)$ or 8.699 MeV $(5/2^+)$ [38], because the energy uncertainty in this lowest energy region is quite large.

The 9.20-MeV resonance was initially introduced by Wiescher *et al.* [37] in their analysis of the ^{10}B(p,γ) reaction measurement. Although a large total width of $\Gamma_{tot} = 500$ keV was incorporated in the analysis of Ref. [37], our calculation with a large Γ_{p0} resulted in diminishing the peak height, and a large $\Gamma_{\alpha 0}$ far exceeding the Wigner limit becomes necessary. In the best fit, Γ_{p0} was assumed to be 0.

For the 8.90-MeV bump, a resonance with $l_\alpha = 3$ gives a good fit, and $J^\pi = 9/2^+$ was the best among them. Other possible J^π values were $3/2^+$, $5/2^+$, and $7/2^+$. The resonance in this energy region may enhance the astrophysical ^{7}Be(α,γ) reaction rate, as shown later. However, it is difficult to derive conclusive resonance parameters with such small peaks broadened by the energy resolution, averaged for a broad range of angles. The current R-matrix calculation could be deceptive at the edge of our energy range. Therefore, it is desirable to perform another study for the resonances in this energy region.

B. Peak around 10 MeV

The α_0 spectrum exhibits a peak, which could be well reproduced by a resonance around 10.0 MeV having a large $\Gamma_{\alpha 0}$.

Four resonances at 9.65, 9.78, 9.97, and 10.083 MeV are known in this region [36]. The 9.78- and 10.083-MeV resonances have been observed in many experiments. The former was seen in ^{10}B(p,γ) [8,39] and ^{10}B(p,α) reactions [8–14], and the latter in ^{10}B(p,α) [8–11,14] and ^{10}B(d,n) reactions [15]. However, the J^π value was controversial for the former state [9,15] while being firmly determined as $7/2^+$ for the latter one.

The current J^π assignments in this region were mostly determined by Wiescher *et al.* [37]. They made tentative assignments of J^π for the three states at 9.65, 9.78, and 9.97 MeV as $3/2^-$, $5/2^-$, and $7/2^-$, respectively, by using an analysis of the ^{10}B(p,γ) reaction measurement data. The 9.65- and 9.97-MeV states, which had not been known before, were introduced to reproduce their excitation functions. Later, a resonance near 9.97 MeV was also observed by the ^{12}C(p,d) reaction [40], but J^π was not determined. No other observation of the 9.65-MeV resonance is known. The 9.65-MeV $(3/2^-)$, 9.78-MeV $(5/2^-)$, and 10.083-MeV $(7/2^+)$ states have candidates of their mirrors at 10.26, 10.34, and 10.60 MeV in ^{11}B, while the 9.97-MeV state has none.

We fully adopted the tentative J^π assignments in [37]. The absence of this resonance in the present p_0 spectrum and previous ^{10}B(α,p) measurements suggests that this 9.97-MeV resonance should have a much smaller Γ_{p0} than the neighboring 9.78- and 10.083-MeV resonances. There is a peak around 9.97 MeV also in the α_1 spectrum, and we introduced $\Gamma_{\alpha 1}$ in the calculation to reproduce the peak.

C. Doublet at 10.5–11.0 MeV

A peak was observed in the p_0 spectrum, as previously observed in the inverse reaction [11,12,15]. There is a peak in the α_0 spectrum at the same $E_{c.m.}$, and the spectral shape suggests that it may be forming a doublet with another resonance at 11.0 MeV. For the higher component in the doublet, a good fit was obtained by using an $l_\alpha = 2$ resonance with $J^\pi = 5/2^-$ or $7/2^-$.

A resonance at 11.03 MeV had been observed in ^{11}B$(^3$He, $t)$ [41], ^{13}C(p,t) [42], and others [38]. However, J^π has not been determined and the resonance is only assumed as a state with an isospin $T = 1/2$.

In the p_1 spectrum, a resonance was observed around 11.03 MeV as the only peak structure in the spectrum. This resonant shape could be reproduced by introducing a resonance with $J^\pi = (3/2^-,\ 5/2^-,\ 7/2^-)$, but the peak height was significantly lower, when J^π was assumed to be $3/2^-$. There is a small peaklike structure also in the α_1 spectrum. The peak is consistent with a calculation introducing a $J^\pi = 5/2^-$ resonance, although the agreement in the peak height is not obvious due to the large uncertainty. In a calculation with $J^\pi = 7/2^-$, $l_{\alpha 1} = 4$ was required for the ^{7}Be $+ \alpha_1$ channel, and a good fit was not obtained. Here we adopt $J^\pi = 5/2^-$ as the best assignment, but $J^\pi = 7/2^-$ might be

also possible, if we ignore the α_1 spectrum, which has quite low statistics.

D. Structure at 11.4 MeV

A small enhancement of the cross section was identified at 11.4 MeV in the α_1 spectrum. A resonance at 11.44 MeV was observed by Jenkin *et al.* [12] in the ^{10}B$(p,\alpha_1)^7$Be* reaction only at forward scattering angles, but the resonance was not clearly seen in the ^{10}B$(p,\alpha_0)^7$Be reaction. Their cross section of the ^{10}B$(p,\alpha_1)^7$Be* reaction was simply decreasing as $\theta_{\rm lab}$ increases. The implication of this angular dependence was not discussed in detail. An R-matrix calculation with a single resonance cannot reproduce such an angular dependence that is asymmetric with respect to $\theta_{\rm c.m.} = 90^\circ$. However, a resonance with a spin $J = 3/2$–$7/2$ can have a feature that the cross section decreases at backward angles toward $\theta_{\rm c.m.} = 180^\circ$.

In the present p_0 spectrum, we did not clearly observe the resonance either. This suggests that the resonance should have a relatively large $\Gamma_{\alpha 1}$. Considering the absence of a sharp peak in the α_0 and p_0 spectrum and the best R-matrix fitting for the α_1 spectrum, we tentatively assigned J^π as $3/2^+$, but $J^\pi = 3/2^-, 5/2^\pm$, and $7/2^\pm$ might be possible. Note that this resonance in the α_0 spectrum is closely located to the sharp peak in the background contribution as shown in Fig. 4, and a small-scale structure could be lost.

E. Doublet at 12–13 MeV

In this energy region, we observed a double-peak structure in the α_0 spectrum with a large cross section.

Not including isospin $T = 3/2$ states, resonances at 12.4 and 12.65 MeV have been known previously. In a previous ^{10}B$(p,\alpha)^7$Be reaction measurement [12], a broad resonance having a large width of 400 keV was observed. By assuming a single level at 12.65 MeV, J^π was tentatively determined as $7/2^+$. The 12.4-MeV resonance was observed in the ^{10}B(p,γ) reaction [43] and in the ^{12}C$(^3$He$,\alpha)$ reaction. In [43], the width was determined as 1–2 MeV and it was discussed as part of a giant resonance.

In the present work, the observed double-peak structure was fitted by using the $7/2^+$ resonance at 12.65 MeV and another resonance at 12.4 MeV. The best fit was made with $J^\pi = 9/2^+$ for the 12.4-MeV resonance. The fit was unsatisfactory using any other J^π, although it was considered as a negative-parity state in [43]. Freer *et al.* [26] also explained this structure as a doublet consisting of $9/2^+$ and $7/2^+$ resonances, although the doublet is displaced in energy by several 100 keV, and the ordering is reversed. The broad peak we observed in the p_0 spectrum at the same energy was also fitted by the doublet of the same two states.

VI. DISCUSSION

A. α-cluster bands

The strong resonances we have observed in the α_0 spectrum have large $\Gamma_{\alpha 0}$, which reflect their α-cluster structure. Figure 9

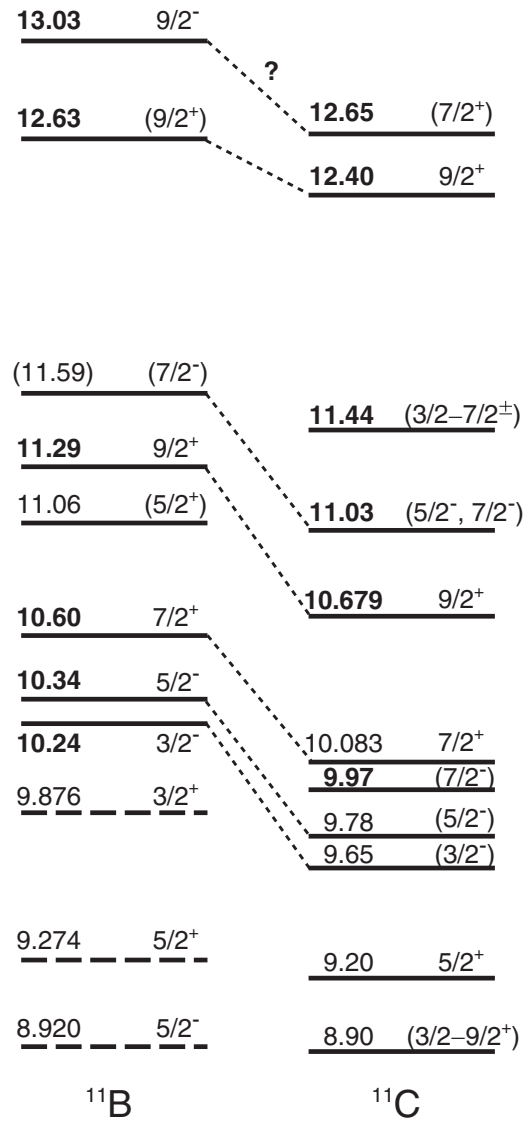

FIG. 9. Resonant states observed in the present work and our previous work [25]. $E_{\rm ex}$ in MeV and J^π in our works are shown for each state, and the states with an $E_{\rm ex}$ in bold letters were observed as significant resonant peaks. The states with dashed lines were not observed in our measurements but are taken from [38].

shows resonant states in ^{11}B and ^{11}C observed in the present work and our previous work [25]. We can identify several pairs of mirror states, as indicated in the figure. The difference in $E_{\rm ex}$ is about 500 keV for the lower pairs of states and smaller for the highest two. Such an energy difference between mirror states was discussed in [26] in relation to the phase transition from shell-model states to cluster states [44,45].

Rotational bands in ^{11}B and ^{11}C, which might be related to the cluster structure, had been discussed in [23,24]. In our previous work [25], we have indicated that the 12.63-MeV resonance in ^{11}B may have $J^\pi = 9/2^+$, as initially mentioned in [24]. We also proposed a new negative-parity band, the head of which is the 8.56-MeV ($J^\pi = 3/2^-$) state. According to a recent calculation based on the antisymmetrized molecular dynamics (AMD) method [46], this can be interpreted as a

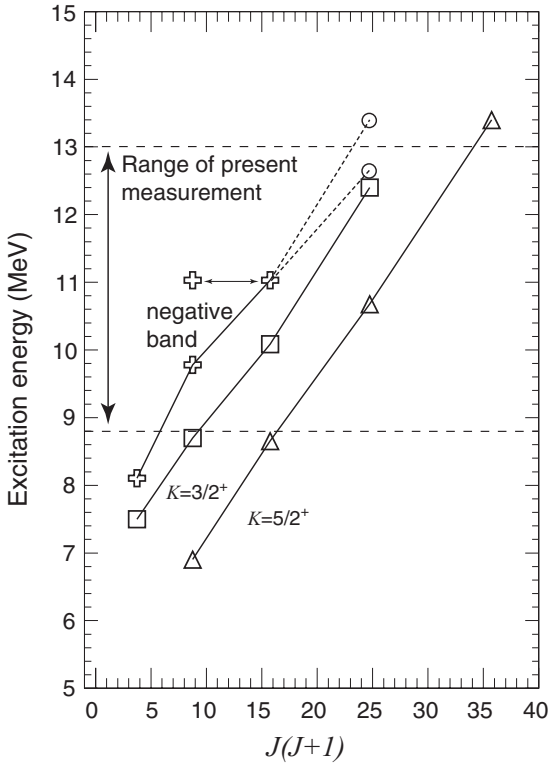

FIG. 10. Two positive-parity rotational bands in ^{11}C suggested in [24], and a newly proposed negative-parity band.

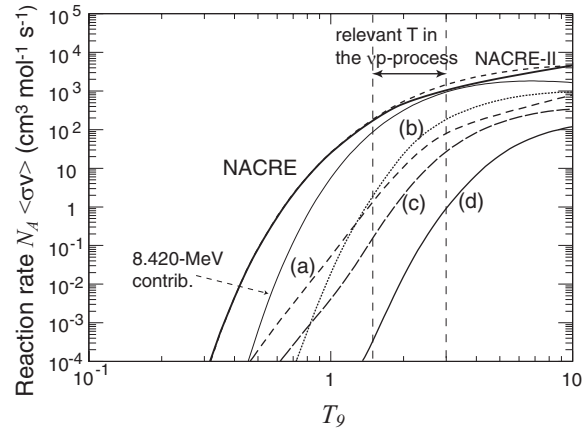

FIG. 11. Resonant reaction rate of ^{7}Be(α,γ) for the 8.90-, 9.20-, and 9.97-MeV resonances, calculated by using the analytical formula (see text and Table II for the labels). The evaluation by NACRE and NACRE-II are shown for comparison. The contribution by the 8.420-MeV resonance, included in NACRE, is also shown.

negative-parity band having a large $B(E2)$ of 20–30 e^2 fm^4, and the members should have a 2α-t cluster structure. The energy of the bandhead appeared as lower than the line expected from the other members, in both the experiment and theory. In [46], the lowering in the level energy was attributed to the relatively weak interactions between 2α-t in the 8.56-MeV state, making a deviation from the higher states, which have a more rigid structure.

A similar discussion can be applied to ^{11}C. Two positive-parity rotational bands, $K = 3/2^+$ and $5/2^+$, were suggested in [24]. We observed a strong resonance with $J^\pi = 9/2^+$ at 12.4 MeV in ^{11}C, and it could be the missing member of the $K = 3/2^+$ rotational band. We propose a new negative-parity band also in ^{11}C, as shown in Fig. 10. The members of the band could have a 2α-^{3}He cluster structure. The head is the 8.10-MeV ($J^\pi = 3/2^-$) state, the mirror of the 8.56-MeV state in ^{11}B. The second member is the 9.78-MeV state, assigned as $J^\pi = 5/2^-$ previously. The third member could be the state at 11.03 MeV. Our assignment was either $J^\pi = 5/2^-$ or $7/2^-$, and the latter assignment agrees with the systematics of this negative band. The systematics predicts that there can be a $J^\pi = 9/2^-$ state around 13 MeV. A candidate is the 12.65-MeV state. In the present work, this state was regarded as forming a doublet together with the 12.4-MeV state. A similar doublet was observed in the mirror nucleus [25], and the higher state was considered to have $J^\pi = 9/2^-$ (see Fig. 9). If the tentative assignment of $J^\pi = 7/2^+$ was wrong, the 12.65-MeV state may have $J^\pi = 9/2^-$, as in the mirror nucleus. Another candidate is the resonance at 13.4 MeV [38], which is known to have a certain α width, but its J^π value has not been determined. In Fig. 10, these states are shown as circles and connected as dotted lines under the assumption that they have $J^\pi = 9/2^-$. The energy of the bandhead (8.10 MeV) appears lower than the systematics would predict from the higher state. This lowering is in agreement with the mirror state [25,46].

A problem is that the $\Gamma_{\alpha 0}$ of the 9.78-MeV ($5/2^-$) resonance is not large, while the neighboring 9.97-MeV resonance with $J^\pi = 7/2^-$ has a larger $\Gamma_{\alpha 0}$, being more likely to be an α-cluster state. The previous studies in the mirror nucleus [25,38] show there is no such corresponding state with $J^\pi = 7/2^-$ in ^{11}B, as shown in Fig. 9. In this respect, the current identification of the resonances and the J^π assignments for $E_{\rm ex} = 9.5$–10 MeV can be questioned.

B. Astrophysical reaction rate of ^{7}Be(α,γ)

The resonances observed in the present work might contribute to the astrophysical ^{7}Be$(\alpha,\gamma)^{11}$C reaction rate at high temperature, $T_9 > 1.5$. Here we calculate the resonant reaction rate and compare it with the total reaction rate evaluated in NACRE [47,48]. In the evaluation in NACRE, only two resonances at 8.1045 and 8.420 MeV are included. These two resonances dominate the reaction rate $N_{\rm A}\langle\sigma v\rangle$ up to the temperature $T_9 \sim 3$, and a Hauser-Feshbach calculation rate was included for the higher temperature.

The resonant reaction rates were calculated for three resonances by using the analytical formula described in [47], and the results are plotted in Fig. 11. The total reaction rate evaluated by NACRE and its recently updated rate (NACRE-II) [48] are also shown for comparison. Table II shows the parameters we used in the calculation. The Γ_γ values and the decay scheme are experimentally unknown for this energy range. Therefore, we evaluated Γ_γ by a calculation based on the Weisskopf unit with a spectroscopic factor of 0.1, which roughly reproduces the experimentally known Γ_γ values of the 8.1045- and 8.420-MeV resonances. Note that such a spectroscopic factor was not explicitly used in the plot of

TABLE II. Parameters used in the reaction rate calculation. The dominant destination states of the γ decay according to our calculation are also shown.

	E_{ex}	J^π	Γ_{tot} (keV)	Γ_α (keV)	Γ_γ (eV)	ω	$\omega\gamma$ (eV)	Dominant destination
(a)	8.90	$9/2^+$	8	8	0.48	2.5	1.2	8.655 MeV ($7/2^+$)
(b)	8.90	$3/2^+$	8	8	1.7	1.0	1.7	ground ($3/2^-$)
(c)	9.20	$5/2^+$	500	13	34	1.5	1.3	ground ($3/2^-$)
(d)	9.97	$7/2^-$	218	153	0.97	2.0	1.4	6.90 MeV ($5/2^+$)

our previous publication [25]. The labels (a)–(d) in Fig. 11 correspond to the ones in Table II. (a) is for our newly identified resonance at 8.90 MeV. J^π was taken to be $9/2^+$ from our best fit. Since the J^π assignment may not be correct, we also evaluated the contribution for the same resonance, but when the resonance had a lower spin of $3/2$, shown as (b). Basically, (b) contributes to the reaction rate more, but its tail contribution is smaller than that of (a). For $T_9 = 2$–3, where the 8.420-MeV resonance dominates the reaction rate, the contribution of the 8.90-MeV resonance was evaluated as around 10% of the total reaction rate. (c) is for the 9.20-MeV resonance, where we also found a small peak in the α_0 spectrum. We used $J^\pi = 5/2^+$ and $\Gamma_{tot} = 500$ keV from previous measurements, although such a large Γ_{tot} was inconsistent with our R-matrix analysis. (d) is for the 9.97-MeV resonance, which was identified as a strong α resonance in the α_0 spectrum. The tentative assignment of $J^\pi = 7/2^-$ [37] was used for the evaluation, and a smaller contribution was obtained, as shown in Fig. 11. We also evaluated contributions for higher resonances, but none of them had an effect as much as or larger than that of case (d).

In summary, the resonances at 8.90 and 9.20 MeV can possibly give significant contributions to the reaction rate for $T_9 = 1.5$–3, although they are unlikely to be more than the contribution of the 8.420-MeV resonance, which dominates the reaction rate. Given that the Γ_γ used here could be underestimated by factors and the decay widths and J^π are also uncertain, more studies are favored for the determination of resonant parameters in the energy region of $E_{ex} = 8.5$–9.5 MeV, which might be difficult to access from the $^{10}B + p$ channel. On the other hand, the resonances above 9.5 MeV can be considered as negligible for $T_9 < 10$.

VII. SUMMARY

We have studied resonant states for $E_{ex} = 8.7$–13.0 MeV in ^{11}C via α-resonant elastic scattering with the thick-target method in inverse kinematics, using a low-energy ^{7}Be beam at CRIB.

We obtained excitation functions of ^{7}Be(α,α_0)^{7}Be, ^{7}Be(α,α_1)^{7}Be*, ^{7}Be(α,p_0)^{10}B, and ^{7}Be(α,p_1)^{10}B* simultaneously, by measuring γ rays in coincidence with α particles or protons. The excitation function of the elastic scattering exhibited strong α resonances, mostly in agreement with previous measurements, and we brought new information on the resonance parameters with an R-matrix analysis. The ^{7}Be(α,p_0)^{10}B excitation function was consistent with the previous measurement of the inverse reaction, ^{10}B(p,α)^{7}Be. The excitation functions were compared with the ones from a similar measurement performed recently [26], and we found differences in the absolute cross section and the energy, although their spectral shapes had a similarity.

A new negative-parity band, which could have a 2α-^{3}He cluster structure, is proposed in ^{11}C, in accordance with the previously proposed band in the mirror nucleus ^{11}B. The resonant contribution for the astrophysical reaction rate of ^{7}Be(α,γ)^{11}C was evaluated at high temperature using the new resonance parameters, and a 10%-order enhancement over the evaluation by NACRE could be expected for $T_9 = 1.5$–3.

ACKNOWLEDGMENTS

The experiment was performed at the RIBF operated by RIKEN Nishina Center and CNS, the University of Tokyo. We are grateful to the RIKEN and CNS accelerator staff for their help. We truly appreciate Prof. Y. K. En'yo and Mr. T. Suhara for useful discussions and suggestions based on their theoretical calculations. This work was partly supported by JSPS KAKENHI (Grant No. 21340053) and a Grant-in-Aid for the Global COE Program "The Next Generation of Physics, Spun from Universality and Emergence" from the Ministry of Education, Culture, Sports, Science and Technology (MEXT) of Japan. One of us (LHK) wishes to acknowledge support from Vietnam National Foundation for Science and Technology (NAFOSTED) under Contract No. 103.04.54.09.

[1] M. Wiescher, J. Görres, S. Graff, L. Buchmann, and F.-K. Thielemann, Astrophys. J. **343**, 352 (1989).
[2] G. M. Fuller, S. E. Woosley, and T. A. Weaver, Astrophys. J. **307**, 675 (1986).
[3] M. Hernanz, J. José, A. Coc, and J. Isern, Astrophys. J. **465**, L27 (1996).
[4] D. Thomas, D. N. Schramm, K. A. Olive, G. J. Mathews, B. S. Meyer, and B. D. Fields, Astrophys. J. **430**, 291 (1994).
[5] A. Coc, S. Goriely, Y. Xu, M. Saimpert, and E. Vangioni, Astrophys. J. **744**, 158 (2012).
[6] S. Wanajo, H.-T. Janka, and S. Kubono, Astrophys. J. **729**, 46 (2011).
[7] C. Fröhlich *et al.*, Astrophys. J. **637**, 415 (2006).
[8] S. E. Hunt, R. A. Pope, and W. W. Evans, Phys. Rev. **106**, 1012 (1957).
[9] A. B. Brown, C. W. Snyder, W. A. Fowler, and C. C. Lauritsen, Phys. Rev. **82**, 159 (1951).

[10] G. B. Chadwick, T. K. Alexander, and J. B. Warren, Can. J. Phys. **34**, 381 (1956).
[11] J. W. Cronin, Phys. Rev. **101**, 298 (1956).
[12] J. Jenkin, L. Earwaker, and E. Titterton, Nucl. Phys. **50**, 516 (1964).
[13] P. Paul, N. Puttaswamy, and D. Kohler, Phys. Rev. **164**, 1332 (1967).
[14] H. Allan, M. Govindjee, and N. Sarma, Proc. Phys. Soc. A **69**, 350 (1956).
[15] J. C. Overley and W. Whaling, Phys. Rev. **128**, 315 (1962).
[16] J. W. Olness, E. K. Warburton, D. E. Alburger, and J. A. Becker, Phys. Rev. **139**, B512 (1965).
[17] H. J. Hauser, M. Walz, F. Weng, G. Staudt, and P. K. Rath, Nucl. Phys. A **456**, 253 (1986).
[18] G. Hardie, B. W. Filippone, A. J. Elwyn, M. Wiescher, and R. E. Segel, Phys. Rev. C **29**, 1199 (1984).
[19] A. Tohsaki, H. Horiuchi, P. Schuck, and G. Röpke, Phys. Rev. Lett. **87**, 192501 (2001).
[20] Y. Kanada-En'yo, Phys. Rev. C **75**, 024302 (2007).
[21] T. Kawabata *et al.*, Phys. Rev. C **70**, 034318 (2004).
[22] T. Kawabata *et al.*, Phys. Lett. B **646**, 6 (2007).
[23] I. Ragnarsson, S. Åberg, H.-B. Håkansson, and R. Sheline, Nucl. Phys. A **361**, 1 (1981).
[24] N. Soić *et al.*, Nucl. Phys. A **742**, 271 (2004).
[25] H. Yamaguchi, T. Hashimoto, S. Hayakawa, D. N. Binh, D. Kahl, S. Kubono, Y. Wakabayashi, T. Kawabata, and T. Teranishi, Phys. Rev. C **83**, 034306 (2011).
[26] M. Freer *et al.*, Phys. Rev. C **85**, 014304 (2012).
[27] S. Kubono *et al.*, Eur. Phys. J. A **13**, 217 (2002).
[28] Y. Yanagisawa *et al.*, Nucl. Instrum. Methods Phys. Res., Sect. A **539**, 74 (2005).
[29] K. P. Artemov *et al.*, Sov. J. Nucl. Phys. **52**, 408 (1990).
[30] H. Yamaguchi, Y. Wakabayashi, G. Amadio, S. Hayakawa, H. Fujikawa, S. Kubono, J. He, A. Kim, and D. Binh, Nucl. Instrum. Methods Phys. Res., Sect. A **589**, 150 (2008).
[31] H. Kumagai, A. Ozawa, N. Fukuda, K. Sümmerer, and I. Tanihata, Nucl. Instrum. Methods Phys. Res., Sect. A **470**, 562 (2001).
[32] A. Alexandrov, I. Alexandrova, S. Podshibyakin, Y. Pyatkov, A. Slyusarenko, A. Shemetov, V. Gayshan, V. Kogan, and V. Pikul, Nucl. Instrum. Methods Phys. Res., Sect. A **312**, 542 (1992).
[33] G. Poggi, M. Bini, P. DelCarmine, F. Meucci, A. Olmi, A. Stefanini, and N. Taccetti, Nucl. Instrum. Methods Phys. Res., Sect. B **119**, 375 (1996).
[34] J. Ziegler, J. Biersack, and M. Ziegler, *SRIM: The Stopping and Range of Ions in Matter* (Lulu, Raleigh, NC, 2008).
[35] N. Larson, *A Code System for Multilevel R-Matrix Fits to Neutron Data Using Bayes' Equations, ORNL/TM-9179/R5* (2000) (unpublished).
[36] F. Ajzenberg-Selove, Nucl. Phys. A **506**, 1 (1990).
[37] M. Wiescher *et al.*, Phys. Rev. C **28**, 1431 (1983).
[38] D. Tilley, J. Kelley, J. Godwin, D. J. Millener, J. E. Purcell, C. G. Sheu, and H. R. Weller, Nucl. Phys. A **745**, 155 (2004).
[39] R. B. Day and T. Huus, Phys. Rev. **95**, 1003 (1954).
[40] G. R. Smith *et al.*, Phys. Rev. C **30**, 593 (1984).
[41] B. A. Watson, C. C. Chang, and M. Hasinoff, Nucl. Phys. A **173**, 634 (1971).
[42] W. Benenson, E. Kashy, D. H. Kong-A-Siou, A. Moalem, and H. Nann, Phys. Rev. C **9**, 2130 (1974).
[43] H. Kuan, M. Hasinoff, W. O'Connell, and S. Hanna, Nucl. Phys. A **151**, 129 (1970).
[44] N. Itagaki, H. Masui, M. Ito, and S. Aoyama, Phys. Rev. C **71**, 064307 (2005).
[45] N. Itagaki, H. Masui, and J. Cseh, J. Phys.: Conf. Ser. **111**, 012006 (2008).
[46] T. Suhara and Y. Kanada-En'yo, Phys. Rev. C **85**, 054320 (2012).
[47] C. Angulo *et al.*, Nucl. Phys. A **656**, 3 (1999).
[48] Y. Xu, K. Takahashi, S. Goriely, and M. Arnould, AIP Conf. Proc. **1377**, 463 (2011).